Magnetic field induced switching of the antiferromagnetic order parameter in thin films of magnetoelectric chromia

Lorenzo Fallarino, Andreas Berger, and Christian Binek

Phys. Rev. B **91**, 054414 — Published 19 February 2015

DOI: 10.1103/PhysRevB.91.054414

Magnetic field-induced switching of the antiferromagnetic order parameter in thin films of magnetoelectric chromia

Lorenzo Fallarino[1], Andreas Berger[1], and Christian Binek[1,2*]

[1]*CIC Nanogune Consolider, Tolosa Hiribidea 76, 20018 Donostia-San Sebastian, Spain*

[2] *Department of Physics & Astronomy and Nebraska Center for Materials and Nanoscience, University of Nebraska, Lincoln, Nebraska 68588-0111, USA*

A Landau-theoretical approach is utilized to model the magnetic field-induced reversal of the antiferromagnetic order parameter in thin films of magnetoelectric antiferromagnets. A key ingredient of this peculiar switching phenomenon is the presence of a robust spin polarized state at the surface of the antiferromagnetic films. Surface or boundary magnetization is symmetry allowed in magnetoelectric antiferromagnets and experimentally established for chromia thin films. It couples rigidly to the antiferromagnetic order parameter and its Zeemann energy creates a pathway to switch the antiferromagnet via magnetic field application. In the framework of a minimalist Landau free energy expansion, the temperature dependence of the switching field and the field dependence of the transition width are derived. Least-squares fits to magnetometry data of (0001)-textured chromia thin films strongly support this model of the magnetic reversal mechanism.

I. Introduction

Phase transitions are among the most challenging and fascinating phenomena in statistical physics [1, 2]. Their investigation sparked the development of concepts and techniques, which find use in many branches of modern physics. Prime examples are spontaneous symmetry breaking, the existence of Nambu-Goldstone modes, and techniques employed in renormalization group theory [3] impacting statistical physics and high energy physics alike [4,5]. In statistical physics of many-body interaction, a critical temperature, T_c, can exist where spontaneous symmetry breaking takes place. It is accompanied by singularities in thermodynamic response functions such as susceptibility and heat capacity. At T_c, non-analytic behavior of the free energy emerges in the thermodynamic limit as a rare exception from the rule that most functions in physics in general and thermal physics in particular can be differentiated to arbitrary order [6,7].

The Landau theory is perhaps the simplest approach to model phase transitions and critical phenomena. It introduces the concept of an order parameter, η, which determines the critical part of the Helmholtz free energy, $F(\eta, T)$. A Legendre transformation from F to the Gibbs free energy $G(h, T) = F(\eta, T) - h\eta$ defines the conjugate field, h. For a simple ferromagnet, the order parameter is the magnetization, M, the conjugate field is the homogenous applied magnetic field H, and $-h\eta = -HM$ is the Zeemann energy. At temperatures $T < T_c$, M can be isothermally switched with the help of H between negative and positive saturation magnetization. This potentially hysteretic switching of the order parameter in response to its conjugate field is a special manifestation of a first-order phase transition [8,9].

In antiferromagnets, where η is determined by the difference between the alternating magnetization of two or more sublattices, there is no direct coupling between H and η. As a result, η neither switches sign in response to H nor is the critical behavior changing in moderate H-fields. AF order is merely weakened due to the presence of H resulting in a shift of the critical temperature to lower values with increasing magnitude of H. The H-field is therefore labeled an irrelevant variable in the renormalization group sense [10] in contrast to the conjugate field, h, which destroys criticality and enables isothermal reversal of η.

In this work, we present and interpret our experimental findings in thin films of magnetoelectric antiferromagnets, based upon a Landau theory approach. For this, we modify the conventional

Landau free energy expansion of bulk antiferromagnets to accommodate for the peculiar surface magnetic properties of magnetoelectric antiferromagnets. The adapted Landau theory is in agreement with our experiments on thin films of magnetoelectric antiferromagnets, which show that η can be switched by sole means of an applied homogeneous magnetic field.

Magnetoelectricity is the specific property of a certain class of antiferromagnets, which enables this peculiar magnetic state and switching phenomenon. The linear magnetoelectric effect relates an applied electric field, $\underline{E}$, with induced magnetization, $\underline{M}$, according to $\mu_0 \underline{M} = \underline{\underline{\alpha}}\, \underline{E}$, where $\underline{\underline{\alpha}}$ is the magnetoelectric susceptibility tensor [11,12,13,14]. Magnetoelectric materials obey specific symmetry requirements. Spatial and time inversion symmetry must be broken individually, however their combined application leaves the spin structure of a magnetoelectric invariant. In magnetoelectric antiferromagnets of finite size then, a boundary magnetization emerges as symmetry allowed surface phenomenon [15,16]. Here translational invariance is broken and transformation properties of the boundary normal vector play a role in the symmetry analysis. Boundary magnetization is an equilibrium property of surfaces or interfaces of magnetoelectric antiferromagnets. It can manifest as a sizable and robust spin-polarization at the boundary of single domain magnetoelectric antiferromagnets. Boundary magnetization has been experimentally evidenced in the archetypical magnetoelectric antiferromagnet α-Cr_2O_3 (chromia) [17,18,19] and recently also in the Fe_2TeO_6 [20]. Note that piezomagnetic and magnetoelectric effects are also symmetry allowed in nano-sized magnetic systems of the ordinary 90 magnetic classes [21,22]. These effects are, however, geometry dependent, typically small in thin films, and scale with the film thickness. They are not responsible for the switching phenomenon reported in our chromia films where boundary magnetization is a well-documented thickness invariant symmetry consequence at surfaces, specifically for systems with linear magnetoelectricity in the bulk [15].

α-Cr_2O_3 belongs to the rhombohedral $R\bar{3}c$ space group, with the *c*-axis as threefold symmetry axis. The inset of Fig.1 shows the schematic corundum-type lattice of chromia [0001] oriented, with the topmost layer made by a hexagonal mesh of Cr^{3+} ions. Below the Néel temperature (T_N=307 K for the bulk), the material adopts an antiferromagnetic (AF) structure, with a magnetic point group $\underline{\bar{3}}\,\underline{m}$.

In bulk crystals of chromia the simultaneous application of an electric and magnetic field can switch the AF spin structure between the two degenerate 180 degree single domain states. The non-linear and hysteretic switching phenomenon has been first reported by Martin and Anderson [23]. More recently, it has been exploited in a chromia based perpendicular exchange bias system to electrically and isothermally switch the exchange bias field [17] and tune the exchange bias training effect [24]. In finite chromia samples, voltage-induced switching of η switches simultaneously the boundary magnetization. In a chromia based exchange bias system, an adjacent ferromagnet can couple via exchange with the boundary magnetization and follow its reversal, hereby giving rise to voltage-controlled switching of exchange bias [17]. Similarly, the linear magnetoelectric effect has been utilized by cooling chromia-based exchange bias heterostructures in the simultaneous presence of electric and magnetic field to below the blocking temperature allowing to select between positive and negative exchange bias [25,26,27].

Recently, we showed through magnetometry of chromia (0001) thin films, that near the AF transition a moderate magnetic field can suffice to select and switch between the two degenerate AF single domain states and their corresponding boundary magnetization [28]. The magnitude of the switching field increases at an exceptional rate upon decreasing the temperature $T < T_N$, which implies potential applications of magnetoelectric antiferromagnets in energy assisted recording media. We suggested that the Zeeman energy of the boundary magnetization makes a sizable contribution to the total magnetic energy of a sufficiently thin film. As a result, a homogeneous magnetic field can reverse the boundary magnetization and with it the rigidly coupled AF order parameter. Here we use a minimalist Landau expansion to derive the functional form for the coercive field, required to reverse the AF order parameter via reversal of the boundary magnetization at a given temperature.

II. Experimental Work

Chromia thin films of d = 26, 50, and 60 nm thickness were deposited by RF magnetron sputtering from a Cr_2O_3 ceramic target (99.99% pure) on polished α-Al_2O_3 (0001) substrates. Prior to deposition, the substrates were ultrasonically cleaned in sequence, first in acetone, then in methanol, and finally in deionized water. All depositions have been carried out at room temperature (RT) by RF-sputtering at a power of 200W in an Ar gas atmosphere of 3.9×10^{-1} Pa. The crystal structure of the films was investigated by out-of-plane symmetrical X-ray diffraction

(XRD) technique using Cu Kα radiation. As-prepared samples showed broad XRD peaks at $2\theta =$ 37.9°, characteristic for the oxygen rich orthorhombic CrO_3 phase with (112) orientation (not shown). The Cr_2O_3 phase is the thermodynamically stable state at temperatures above 500 °C. However, only at T >900 °C epitaxial transformation from CrO_3 to the Cr_2O_3 phase can be achieved for film deposition on top of sapphire substrates [29,30,31,32,33]. Therefore, we thermally annealed our samples after deposition at 1000 °C in vacuum (3 Pa) for 1 h. Fig.1 shows the XRD data for samples of thicknesses d = 26, 50, and 60 nm after the annealing step. In addition to the narrow peak at $2\theta =$ 41.68° originating from Al_2O_3 (0006) reflection, each pattern reveals an intense peak at $2\theta =$ 39.75° with a FWHM of 0.57° (26 nm), 0.54° (50 nm), 0.43° (60 nm), corresponding to the Cr_2O_3 (0006) reflection. We did not observe any XRD-peaks that can be attributed to other crystallographic orientations. The XRD results evidence that thermal treatment transforms the as-prepared films from the CrO_3 phase into chromia with the c-axis normal orientation to the substrate. Visual inspection of the films reveals chromia's characteristic green color indicating virtually perfect stoichiometry. All chromia films have been magnetically characterized using a commercial Quantum Design MPMS 3 SQUID-VSM magnetometer. Its sensitivity suffices to measure magnitude and sign of the boundary magnetic moment of the films which is of the order of only a few 10^{-11}Am^2.

The most common way to characterize a ferromagnetically ordered system is by measuring the magnetic moment, m, in isothermal response to an applied magnetic field, H, resulting in an m vs. H hysteresis loop. In the case of our AF films, characterization via isothermal hysteresis loops is not a viable option because the signal of interest, originating from the BM of a single layer of spins, is weak. Background contributions which appear upon applying magnetic fields easily mask the BM. The most prominent background contributions originate from the diamagnetic susceptibility of the sapphire substrate and the AF bulk susceptibility of chromia. While the former is virtually temperature independent, the latter increases with increasing temperature and maximizes near T_N. Additionally, one might be concerned about the presence of quadrupolar magnetic fields which are known to exist in response to free electric charges embedded in a bulk magnetoelectric [34]. Quadrupolar fields of charged chromia samples have indeed been detected with the help of particularly designed pick-up coils operating in concert with quantum interference detection techniques [35]. However, the magnitude of such fields is typically two orders below the earth magnetic field. Moreover, the gradiometer pick-up coils of

magnetometers, such as the Quantum Design MPMS 3 SQUID-VSM used in our study, are specifically designed to be sensitive to the volume averaged magnetic moment determined from the sample's dipolar stray-field while minimizing the pick-up of higher multipole contributions. In order to avoid masking of the BM signal by secondary effects, we utilize an experimental procedure that allows us to monitor magnetization reversal as a function of temperature rather than magnetic field. Although magnetization reversal is stimulated by an applied reversal field opposing the remanent BM upon heating from 100 K to a target temperature $T^* < T_N$, the actual magnetization measurements are performed at zero applied magnetic field. The protocol insures the absence of paramagnetic and diamagnetic background signals. Details of the temperature and field dependent initial magnetic state preparation and the subsequent zero field measurement protocol have been published elsewhere [28].

Fig.2 shows selected $\langle m \rangle'_T$ vs. T^* curves measured for a reversal field of $\mu_0 H_R$ = -7T for the three thin film samples of 26 nm (triangle), 50 nm (squares) and 60 nm (circles) thickness[1]. The flipping temperature, T_f, indicated by dashed (red) lines in Fig.2, is defined as the temperature where magnetization reversal takes place for a given reversal field $\mu_0 H_R$. It is quantified by the condition $\langle m \rangle'_T = 0$ (see footnote for definition of $\langle m \rangle'_T$). The data in Fig. 2 show that both the position and the sharpness of the magnetization reversal depend on the thickness of the samples. For the thinnest film, a broad transition occurs around T_f = 283.6 K, while for the thickest film, a narrow switching takes place around T_f = 292.1 K. Moreover, our experiments show that T_f and the temperature dependent width, w, of the reversal depend on the strength of the reversal field $\mu_0 H_R$. In an isothermal magnetization reversal at $T = T_f$ (not shown due to complications from background signals much larger than the BM as outlined above) one would identify the reversal field with the coercive field H_C of the hysteresis. We use therefore H_C and H_R synonymously with preference for H_R in the context of our temperature dependent experiments and H_C in the context of the theory.

Fig. 3 displays the square of the measured reversal fields $\mu_0 H_R$ as a function of T_f for the Cr_2O_3 films of d = 26 nm (squares), 50 nm (triangles), and 60 nm thickness (circles). Horizontal bars indicate the width, w, of the transition temperature region [28]. It will be analyzed together with

[1] *In order to improve the signal to noise ratio, the displayed data ,$\langle m \rangle'_T$, represent the numerical temperature integration of the zero field heating m vs T curves,* $\langle m \rangle_T = \frac{1}{50K} \int_{250K}^{300K} m(T) dT$, *normalized to the corresponding maximum integral value, i.e.* $\langle m \rangle'_T = \langle m \rangle_T / (\langle m \rangle_T)_{max}$

the T_f – dependence of the reversal field with the help of the results from the Landau theory outlined next.

III. Theory and Comparison with Experimental Results

III.I. Temperature dependence of the coercive field

Starting point of our consideration is a Landau free energy expansion, *F*, in powers of the AF order parameter, η, and the boundary magnetization, *m*, which couples with η via a bilinear exchange term $E_{ex} = -Jm\eta$ and the applied magnetic field *H* via a Zeemann term $E_Z = -mH$. Note that effects of *H*-induced magnetization as a secondary order parameter in the bulk of the antiferromagnet are neglected [36,37]. Here, for simplicity, we rather focus on the susceptibility of η on *H* mediated through the coupling between η and *m* and between *m* and *H*. This effect dominates in thin films but diminishes with increasing film thickness. The constant *J* quantifies the coupling strength between η and *m*. Its sign controls whether parallel ($J>0$) or antiparallel alignment ($J<0$) between η and *m* is favored. With this minimalist extension of the free energy of bulk antiferromagnets to thin film antiferromagnets with boundary magnetization we obtain

$$F = \frac{1}{2}a_1\,\eta^2 + \frac{1}{4}a_2\,\eta^4 + \frac{1}{2}b_1\,m^2 + \frac{1}{4}b_2 m^4 - Jm\eta - mH. \qquad (1)$$

The parameter a_1 has the usual linear temperature dependence of the form $a_1 = a(T - T_N)$ where T_N is the Néel temperature, and $a > 0$ and $a_2 > 0$ are constants. For the expansion coefficients $b_{1,2}$ we impose only the single assumption that all *m*-dependent terms in the free energy are small in comparison with the η-dependent terms such that in the limit of thick films Eq.(1) becomes the Landau expansion of a bulk antiferromagnet. The superposition of the total free energy from a bulk and a surface contribution, which levels off inversely proportional to the layer thickness, is a standard approach in the study of surface effects for magnetic phase transitions [38].

Similar to the technique used in the case of coupled order parameters known from the Landau theory of metamagnets [36] or improper ferroelectrics [39], we eliminate here the boundary magnetization, *m*, from Eq.(1) with the help of the equilibrium condition $\frac{\partial F}{\partial m} = 0$ which yields

$$-H + b_1 m + b_2 m^3 - J\eta = 0. \qquad (2)$$

Because we aim at compact analytic expressions suitable for intuitive interpretation and useful to fit our experimental data, we simplify Eq.(2) through approximation rather than solving the cubic equation in m. We take advantage of that fact that for all T sufficiently close to T_N, $|b_2 m^3| \ll |b_1 m|$ allowing for an approximate solution of Eq.(2) which reads

$$m = \frac{H+J\eta}{b_1}. \tag{3}$$

As expected, in the absence of an applied field, Eq. (3) fulfills the symmetry condition $m(-\eta) = -m(\eta)$. It implies that the reversal of the boundary magnetization follows the reversal of the AF order parameter and it is consistent with the experimentally observed rigid coupling implying that non-zero boundary magnetization depends on long range AF order. Substitution of Eq.(3) into Eq.(1) yields the free energy expression F_η , which reads

$$F_\eta = -\frac{(H+J\eta)^2}{2b_1} + \frac{b_2(H+J\eta)^4}{4b_1^4} + \frac{1}{4}\left(a_2\eta^4 + 2a\eta^2(T-T_N)\right). \tag{4}$$

Subsequent expansion of F_η up to first order in the small parameters $T_N - T$, J, and H yields

$$F_l = -\frac{J}{b_1}H\eta + \frac{1}{4}(2a\eta^2(T-T_N) + a_2\eta^4). \tag{5}$$

The linearized free energy, F_l, allows for an intuitive understanding of H-induced switching of the AF order parameter.

Fig. 4 shows $F_l(\eta)$ for magnetic fields $H=0$, $H=H_c$ and $H = H_c + \Delta H$ at constant $T < T_N$, and constant values for a, a_2, b_1 and J. At H=0, the free energy is a common symmetric double well potential with two degenerate equilibrium AF order parameters at $\eta_{1,2}^{eq}(T) = \pm\sqrt{\frac{a(T_N-T)}{a_2}}$ reflecting the behavior of a bulk antiferromagnet. The H=0 free energy is an even function. This symmetry is broken for non-zero H. The presence of a magnetic field energetically favors one of the equilibrium AF states over the other. This is a non-trivial consequence of the interplay between Zeemann energy $E_Z = -mH$ and the coupling between m and η. From the perspective of the bulk AF order parameter, the homogeneous H-field is an irrelevant field. Therefore, in the absence of coupling (J=0) or in the limit of bulk-like films, H does neither affect the criticality of the AF phase transition nor does an H-field stabilize a particular AF single domain state.

However, in the presence of coupling, $E_{ex} = -Jm\eta$, an increase in H destabilizes one of the minima of F while energetically favoring the minimum which corresponds to the reversed AF order parameter (see left (right) sketch in Fig 2 for chromia spin structure destabilized (stabilized) in the presence of $H>0$). Ultimately, at $H = H_c$, the destabilized minimum evolves into an inflection point of F characterized by $\frac{\partial^2 F}{\partial \eta^2} = 0$. Here η switches from its reduced value $\eta_c(H_c)$ into the new equilibrium at $\eta_{eq}(H > H_c)$.

Although the free energy landscape and the switching scenario of η in thin films show strong resemblance of field-induced magnetization reversal of a ferromagnet, it is important to remember that in this work, the reversal of an AF order parameter is investigated. In contrast to a ferromagnet where magnetization and H are conjugate variables, the H-field induced reversal of η is non-trivial because the homogeneous H-field and the AF order parameter do not directly couple. In magnetoelectric thin films, reversal of η driven by H is possible only in the presence of boundary magnetization. In the limit of thin films, the m-dependent terms in the free energy make a sufficiently large contribution to the total free energy, even if the surface free energy falls off rather quickly via the inverse thickness dependence. It is worth mentioning that the free energy expansion of Eq.(1) does not take into account higher order effects originating from non-zero AF susceptibility at $T > 0$. As a consequence of thermal excitation, field-induced magnetization in bulk antiferromagnets couples to the H-field with an overall destabilizing effect on AF order. The increase of magnetization resembles increased imbalance between the AF sublattices and therefore a reduction of the AF order parameter. In a simple bulk antiferromagnet at $T > 0$, an H-field applied along the easy axis destabilizes both degenerate equilibrium spin states without lifting the degeneracy between them. The pronounced lowering of the free energy at $\eta_{eq}(H > H_c)$ at $H = H_c + \Delta H$ sketched in Fig. 4 is therefore an overestimation of the stabilization effect and a consequence of neglecting AF susceptibility. Nevertheless, our simple ansatz captures the essentials of the experimentally observed reversal phenomenon.

The primary goal of our Landau theoretical approach is the derivation of an analytic expression $H_c(T_f)$ which allows fitting of the experimental data shown in Fig. 3. Guided by the intuitive discussion of Fig. 4 we apply the condition $\frac{\partial^2 F}{\partial \eta^2} = 0$ to the free energy expression (5). We obtain

the approximate result $\eta_c(T_f) \approx \sqrt{\frac{a(T_N-T_f)}{3a_2}}$ for the magnitude of η at the point of switching. Within the approximation $F \approx F_l$, $\eta_c(T_f)$ is a factor $1/\sqrt{3}$ smaller than $\eta^{eq}(H=0,T_f)$ in agreement with intuitive expectation.

Next we derive $H_c(T_f)$ from the equilibrium condition $\frac{\partial F}{\partial \eta} = 0$. In the framework of an iterative approximation we utilize $\eta_c(T_f) \approx \sqrt{\frac{a(T_N-T_f)}{3a_2}}$ but proceed with the more accurate free energy expression $F \approx F_\eta$ to derive the equation of state

$$-\frac{J(H+J\eta)}{b_1} + \frac{b_2 J(H+J\eta)^3}{b_1^4} + \left(a_2\eta^3 + a\eta(T-T_N)\right) = 0\,. \qquad (6)$$

Evaluating Eq.(6) at $T=T_f$ and substituting $\eta_{cf}(T_f) \approx \sqrt{\frac{a(T_N-T_f)}{3a_2}}$ yields, after linearization in the small coefficient b_1,

$$H_c = -J\eta_c(T_f) + O[b_1]^{\frac{4}{3}} \approx -J\sqrt{\frac{a(T_N-T_f)}{3a_2}}, \qquad (7)$$

where $O[b_1]^{\frac{4}{3}}$ indicates that terms of the order $b_1^{\frac{4}{3}}$ have been neglected. Eq.(7) is used to fit the experimental data shown in Fig. 3.

Fig. 3 shows $\mu_0^2 {H_c}^2$ vs. T_f for the three film thicknesses d = 26 (squares), 50 (triangles), and 60 nm thickness (circles) so that the square of Eq.(7) translates into the linear T_f-dependence of the form $\mu_0^2 {H_c}^2 = \mu_0^2 \frac{J^2 a}{3a_2}(T_N - T_f)$. Lines show best linear fits with $T_N(26nm)$ =293.0 K, $T_N(50nm)$ =295.8 K, and $T_N(60nm)$ =299.1K and $\mu_0^2 \frac{J^2 a}{3a_2} = -5.23$, -5.72, and -7.29 T^2/K.

In order to crosscheck the validity of the analysis above we substitute Eq.(7) into Eq.(3) to derive the magnitude of the boundary magnetization at the reversal point. The substitution reveals $m(H_c) = 0$ in agreement with the intuitive expectation. Because m and η are rigidly coupled, reversal of η requires a change in sign of m with a crossing of the state m=0 at H=H_c.

III.II. Field dependence of the transition width

In addition to the $H_c(T_f)$-dependence displayed in Fig. 3, horizontal bars of the data points quantify the temperature width of the transition for various reversal fields. Next we derive an analytic expression which allows fitting of the experimental transition width, w vs. H_c. Intuitively, the width of the transition is determined by the driving force $f = -\frac{\partial F}{\partial \eta}$, which determines the dynamics of the switching process from the destabilized minimum of the free energy to its global minimum. The switching dynamics could be modeled via the phenomenological Landau-Khalatnikov equation relating f with the temporal change of η [40,41]. From a dynamic perspective it is intuitive that the larger $|f|$ is, the faster the system will relax into the new equilibrium. In a quasi-static experiment this translates into a reduced temperature width, w, of the transition with increasing $|f|$. A force $|f| > 0$ is generated when increasing H from H_c, where f=0 (see lower dashed line in Fig.4 marking the horizontal tangent of $F_l(\eta)$ at η_c) to $H_c + dH$. At $H_c + dH$ a force $|f| > 0$ drives the system into the stable equilibrium (see upper dashed line in Fig. 4 marking a tangent of $F_l(\eta)$ with negative slope at η_c).

Using this intuition picture we motivate from $f(H_c + dH) = f(H_c)\frac{\partial f}{\partial H} = \frac{\partial f}{\partial H}$ the analytic expression for the transition width

$$w \propto \left|\frac{1}{\frac{\partial f}{\partial H}}\right|. \tag{8}$$

Because the temperature and field dependence of w is a higher order effect, the evaluation of $\frac{\partial f}{\partial H}$ needs to be carried out beyond the free energy approximation F_l which is the result of linearization of F_η with respect to J, H, and T. We rather start from F_η given by Eq.(4) and linearize F_η only with respect to J to keep the higher order H and T dependencies. Using $F \approx F_\eta(J = 0) + \frac{\partial F_\eta}{\partial J}J$ to evaluate $\frac{\partial f}{\partial H} = -\frac{\partial}{\partial H}\frac{\partial F}{\partial \eta}$ we obtain $\frac{\partial f}{\partial H} \approx -J(-\frac{1}{b_1} + \frac{3b_2H^2}{b_1^4})$. With this we arrive at a functional form of the transition width which reads

$$w = \frac{w_0}{1-(C\mu_0 H)^2}, \tag{9}$$

with C being a fitting parameter and w_0 the experimentally observed residual finite transition width for $H \to 0$ and $T \to T_N$. The H^2-dependence of w guarantees symmetry in the transition width for switching from positive to negative and negative to positive AF order parameter.

Figure 5 shows the w vs. H_c data for samples of thickness d = 26 (squares), 50 (triangles), and 60 nm thickness (circles). All data sets merge into a common limiting value $w_0 \approx 0.2$ K allowing to fix w_0 for all data sets such that Eq.(8) can be applied as a single parameter fit. The lines are the respective best fits of Eq.(9) with $C(d = 26nm) = 0.132\,T^{-1}$, $C(d = 50nm) = 0.122\,T^{-1}$, and $C(d = 60nm) = 0.105T^{-1}$. Thickness dependent parameter variation is a common feature in thin films. The thickness dependence of the ordering temperature with increasing film thickness is a prominent example [42,43,44]. Here, in a similar manner, the C-parameter decreases systematically with increasing film thickness reflecting the increasing steepness of $H_c(T_f)$ and reduced smearing of the transition towards the bulk limit. In fact, a quantitative relation between the thickness dependence of the C-parameter and $\frac{d\mu_0^2 H_c^2}{dT_f} = -\mu_0^2 \frac{J^2 a}{3a_2}$ is suggested from the virtual thickness invariance of the product, $P = -C\frac{d\mu_0^2 H_c^2}{dT_f}$ with P=0.69, 0.70, and 0.77T/K for d= 26, 50, and 60 nm, respectively, corroborating the consistency of our analysis.

IV. Summary and Conclusion

We have shown that in thin films of magnetoelectric antiferromagnets, with experimental reference to chromia, the presence of robust boundary magnetization can be utilized to switch the antiferromagnetic order parameter between positive and negative registration solely by magnetic means. A minimalist Landau free energy analysis provides analytic expressions for the temperature dependence of the reversal field and the width of the transition. The theoretical results are in excellent agreement with the experimental data and confirm the proposed reversal mechanism. Reversal with the help of a homogeneous magnetic field is based on rigid coupling between the boundary magnetization and the antiferromagnetic order parameter and the Zeemann energy, which couples the boundary magnetization to the applied magnetic field. With increasing film thickness the contribution of the surface terms in the free energy decreases and the reversal mechanism becomes less effective, so that in the bulk limit, reversal of the antiferromagnetic order parameter of magnetoelectric antiferromagnets requires the simultaneous presence of electric and magnetic fields. Our theoretical understanding of antiferromagnetic domain reversal in magnetoelectric thin films via homogeneous magnetic fields has potential application for energy assisted magnetic recording media. Here, the sensitivity of the temperature dependence of the coercive field is a crucial figure of merit for media optimization.

Acknowledgement

We acknowledge funding from the Basque Government under Program No. PI2012-47 and the Spanish Ministry of Economy and Competitiveness under Project No. MAT2012-36844. Ch. Binek gratefully acknowledges support by the Basque Foundation for Science, Ikerbasque, the Semiconductor Research Corporation through the Center for Nanoferroic Devices, an SRC-NRI Center under Task ID 2398.001, Theme 2587.001 and 2398.0001, the National Science Foundation (NSF) through the Nebraska Materials Research Science and Engineering Center (MRSEC) (grant No. DMR-1420645), and the Nebraska Center for Materials and Nanoscience. L. Fallarino thanks the Basque Government for the PhD fellowship (Grants No. PRE_2013_1_974 and No. PRE_2014_2_142).

Figure captions

Fig. 1: θ-2θ XRD spectra for (0001) oriented Cr_2O_3 film samples of 26 nm (upper black line), 50 nm (center red line) and 60 nm (lower blue line) thickness. The inset shows the corundum-type crystal structure of α-Cr_2O_3. Large (green) spheres represent Cr^{3+} ions, small (gray) spheres represent O^{2-} ions.

Fig.2: Average magnetic moment $\langle m \rangle'_T$ vs. T^* (see text) for 26 nm (triangle), 50 nm (squares), and 60 nm (circles) sample thickness, respectively. The (red) dashed lines indicate the condition $\langle m \rangle'_T = 0$ which quantifies the respective flipping temperature T_f. Insets in the middle panel show sketches of chromia's two AF single domain states and their corresponding boundary magnetization. The lower two layers of arrows in each sketch represent the bulk AF spin structure. The top layer on the right (left) side represents positive (negative) boundary magnetization.

Fig. 3: Square of the coercive field, $(\mu_0 H_C)^2$, vs. flipping temperature, T_f, for samples of thickness d=26 nm (squares), 50 nm (triangle), 60 nm thickness (circles). Lines are least-squares fits of Eq.(8) to the data. Horizontal bars quantify the transition width, w, of reversal.

Fig. 4: Plots of the free energy expansion $F_l(\eta)$ according to Eq.(5) for three selected magnetic fields $H=0$, $H=H_c$ and $H = H_c + \Delta H$ at a constant temperature $T<T_N$ and constant values a, a_2, b_1 and J. Dashed vertical lines mark the two equilibrium positions $\eta_{1,2}^{eq}$ of $F_l(\eta)$ for H=0, the position of the inflection point in $F_l(\eta)$ for $H=H_c$ where the AF order parameter is reduced to η_c, and the position of the field stabilized global minimum in $F_l(\eta)$ for

$H = H_c + \Delta H$ where the order parameter takes the value η_{eq}. Dashed tangential lines with zero and negative slope indicate the absence of a gradient in the inflection point for H=H_c and the presence of a finite driving force f for $H = H_c + \Delta H$.

Fig. 5: Temperature width, w, of the transition for samples of thickness d = 26 nm (squares), 50 nm (triangle), 60 nm thickness (circles) as a function of the coercive field. Lines are least-squares fits of Eq.(9) to the experimental data.

References

[1] C. Domb, and M.S. Green, Phase Transitions and Critical Phenomena, Vol. 1-6, New York 1972.
[2] C. Domb, and J. Lebowitz, Phase Transitions and Critical Phenomena, Vol. 7-20, New York, 1973-2001.
[3] K. G. Wilson, Phys. Rev. B 4, 3174 (1971).
[4] T. Brauner, Symmetry 2, 609 (2010).
[5] P.W. Higgs, Phys. Rev. B 13, 508 (1964).
[6] C.N. Yang and T.D. Lee, Phys. Rev. 87 (1952) 404.
[7] T.D. Lee and C.N. Yang, Phys. Rev. 87 (1952) 410.
[8] M. E. Fisher, and A. N. Berker, Phys. Rev. B **26**, 2507 (1982).
[9] K. Binder, Rep. Prog. Phys. **50**, 783 (1987).
[10] R.R. dos Santos, J. Phys. C: Solid State Phys. **18**, L1067 (1985).
[11] I. E. Dzyaloshinskii, Soviet Phys. JETP **10,** 628 (1960).
[12] D. N. Astrov *Soviet Phys. JETP* **11** 708 (1960), *ibid* 1961 **13** 729
[13] T. H. O'Dell, *The Electrodynamics of Magneto-Electric Media*, (North-Holland 1970).
[14] M. Fiebig, J. Phys. D: Appl. Phys. **38**, R123 (2005)
[15] K.D. Belashchenko, Phys. Rev. Lett. **105**, 147204 (2010).
[16] A. F. Andreev, JETP Lett. **63**, 758 (1996).
[17] X. He, Y. Wang, N. Wu, A. N. Caruso, E. Vescovo, K. D. Belashchenko, P. A. Dowben, and Ch. Binek, Nat. Mater. 9, 579 (2010).
[18] N. Wu, X. He, A. L. Wysocki, U. Lanke, T. Komesu, K. D. Belashchenko, Ch. Binek, and P. A. Dowben, Phys. Rev. Lett. **106**, 087202 (2011).
[19] Shi Cao, Xin Zhang, Ning Wu, A T N'Diaye, G Chen, A K Schmid, Xumin Chen, W Echtenkamp, A Enders, Ch Binek, and P A Dowben, New J. Phys. **16**, 073021(2014).
[20] JL. Wang, J. A. Colon Santana, N. Wu, C. Karunakaran, J. Wang, P. A Dowben, and Ch. Binek, J. Phys.: Condens. Matter **26,** 055012 (2014).
[21] Ch. Binek, Ising-type antiferromagnets: Model systems in statistical physics and in the magnetism of exchange bias, Springer Tracts in Modern Physics, 2003, p. 89.
[22] E. A. Eliseev, A. N. Morozovska, M. D. Glinchuk, B. Y. Zaulychny, V. V. Skorokhod, and R. BlincPhys. Rev. B **82**, 085408 (2010).
[23] T. J. Martin, and J. C. Anderson, IEEE Trans. Mag. **2**, 446 (1966).
[24] W. Echtenkamp and Ch. Binek, Phys. Rev. Lett. **111**, 187204 (2013).

[25] Pavel Borisov, Andreas Hochstrat, Xi Chen, Wolfgang Kleemann, and Christian Binek, Phys. Rev. Lett. **94**, 117203 (2005).
[26] T. Ashida, M. Oida, N. Shimomura, T. Nozaki, T Shibata, and M. Sahashi, APL **104**, 152409 (2014)
[27] K. Toyoki, Yu Shiratsuchi, A. Kobane, S. Harimoto, S. Onoue, H. Nomura, and R. Nakatani, J. Appl. Phys. **117**, 17D902 (2015).
[28] L. Fallarino, A. Berger, and Ch. Binek, Appl. Phys. Lett.**104**, 022403 (2014).
[29] S.H. Yang, S.J. Liu, Z.H. Hua, S.G. Yang, J. Alloys Compd. **509**, 6946-6949, (2011).
[30] H. Mashiko, T. Oshima, and A.Ohtomo, Jpn. J. Appl. Phys. **51**, 11PG11 (2012).
[31] V.A. Drebushchak and A. I. Turkin, J. Therm. Anal. Cal. **90**, 795-799 (2007).
[32] F.S. Stone and J. C. Vickerman, Trans. Faraday Soc. **67**, 316-328 (1971).
[33] S. Y. Jeong, J. B. Lee, H. Na, and T. Y. Seong, Thin Solid Films 518, 4813 (2010).
34 M. Fechner, N.A. Spaldin, and I. E. Dzyaloshinskii, Phys. Rev. B **89**, 184415 (2014).
35 D.N. Astrov, N. B. Ermakov, A. S. Borovik-Romanov, E. G. Kolevatov, and V. I. Nizhankoskii, J. Exp. and Theor. Phys. Lett. **63**, 745 (1996).
[36] J.M. Kincaid, E.G.D. Cohen, Phys. Rep. Phys. Lett. C **22**, 57 (1975).
[37] A.F.S. Moreira, W. Figueiredo, and V.B. Henriques, Eur. Phys. J. B **27**, 153 (2002).
[38] D.P. Landau, K. Binder, J. Appl. Phys. **63**, 3077 (1988).
[39] A. P. Levanyuk and D. G. Sannikov, Usp. Fiz. Nauk 112, 561
[40] Ch. Binek, Phys. Rev. B. **70**, 014421 (2004).
[41] Ch. Binek, S. Polisetty, Xi He and A. Berger, Phys. Rev. Lett. **96**, 067201 (2006).
[42] K. Binder, Phys. Rev. Lett. **47**, 693 (1981).
[43] X. He, W. Echtenkamp, and Ch. Binek, Ferroelectrics **426**, 81 (2012).
[44] T. Ambrose and C. L. Chien, Phys. Rev. Lett. **76**, 1743 (1996).

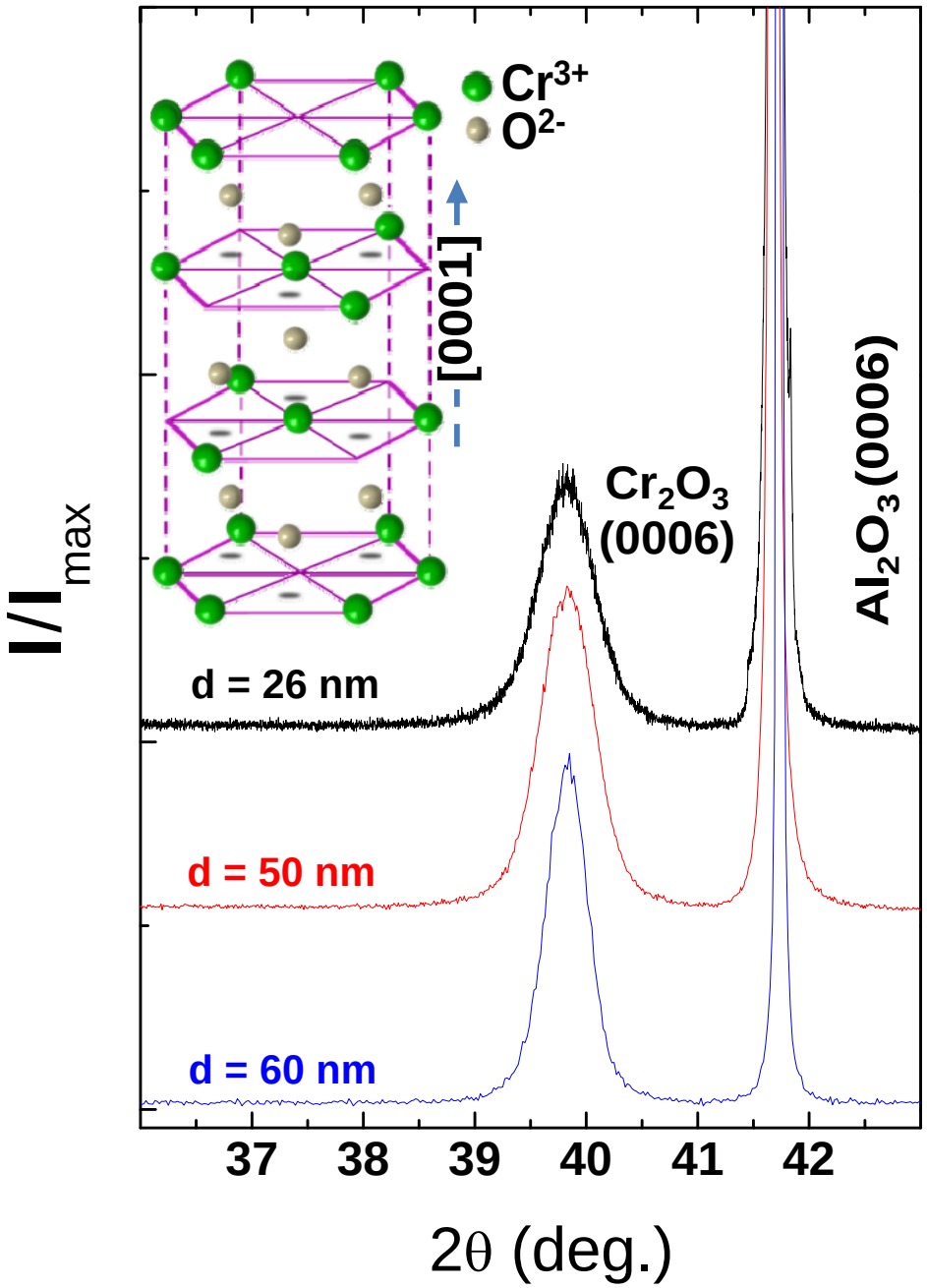
I/I max
Cr3+
O2-
[0001]
Cr2O3
(0006)
Al2O3 (0006)
d = 26 nm
d = 50 nm
d = 60 nm
37
38
39
40
41
42
2θ (deg.)

Fig. 1

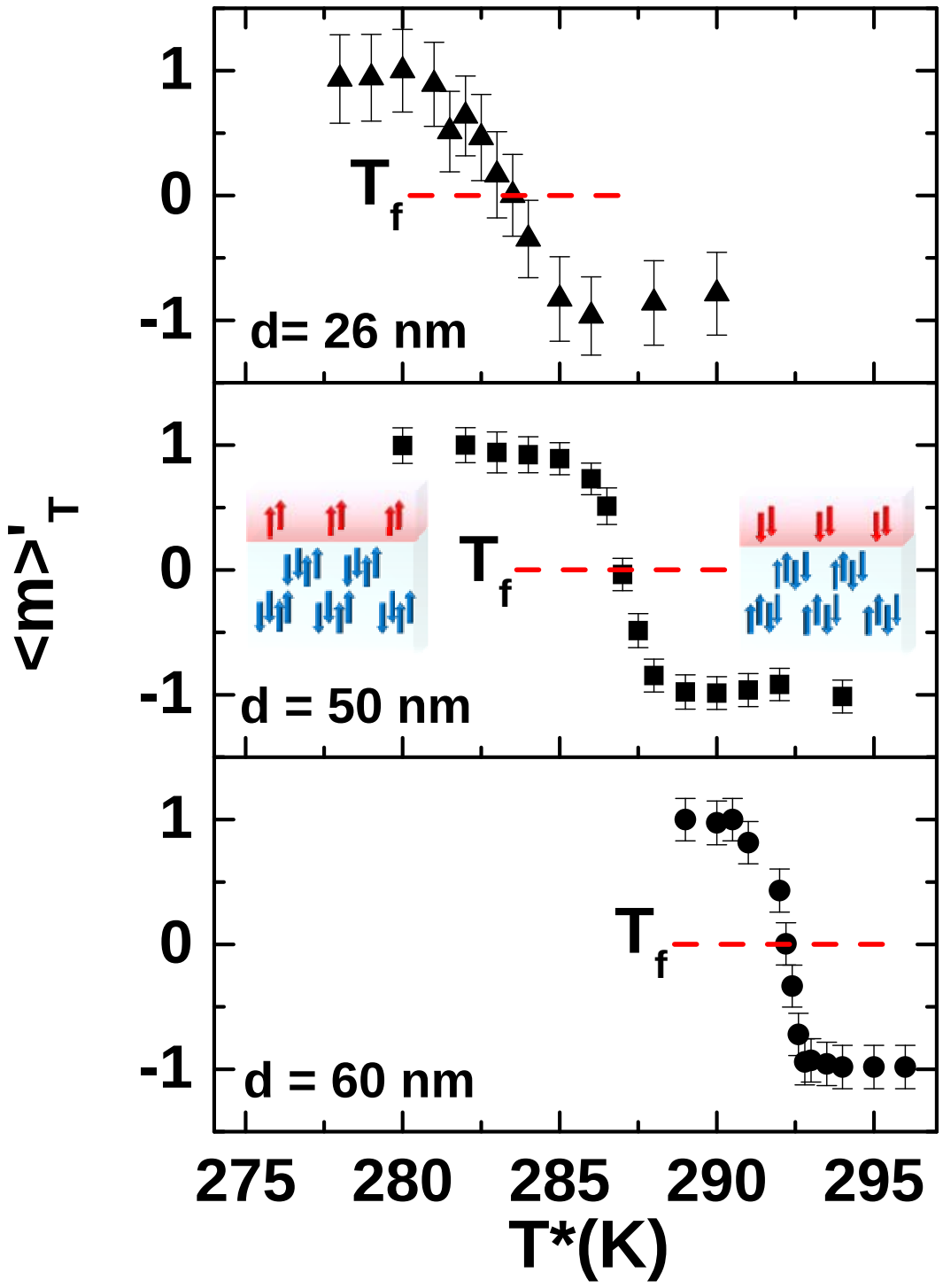

Fig.2

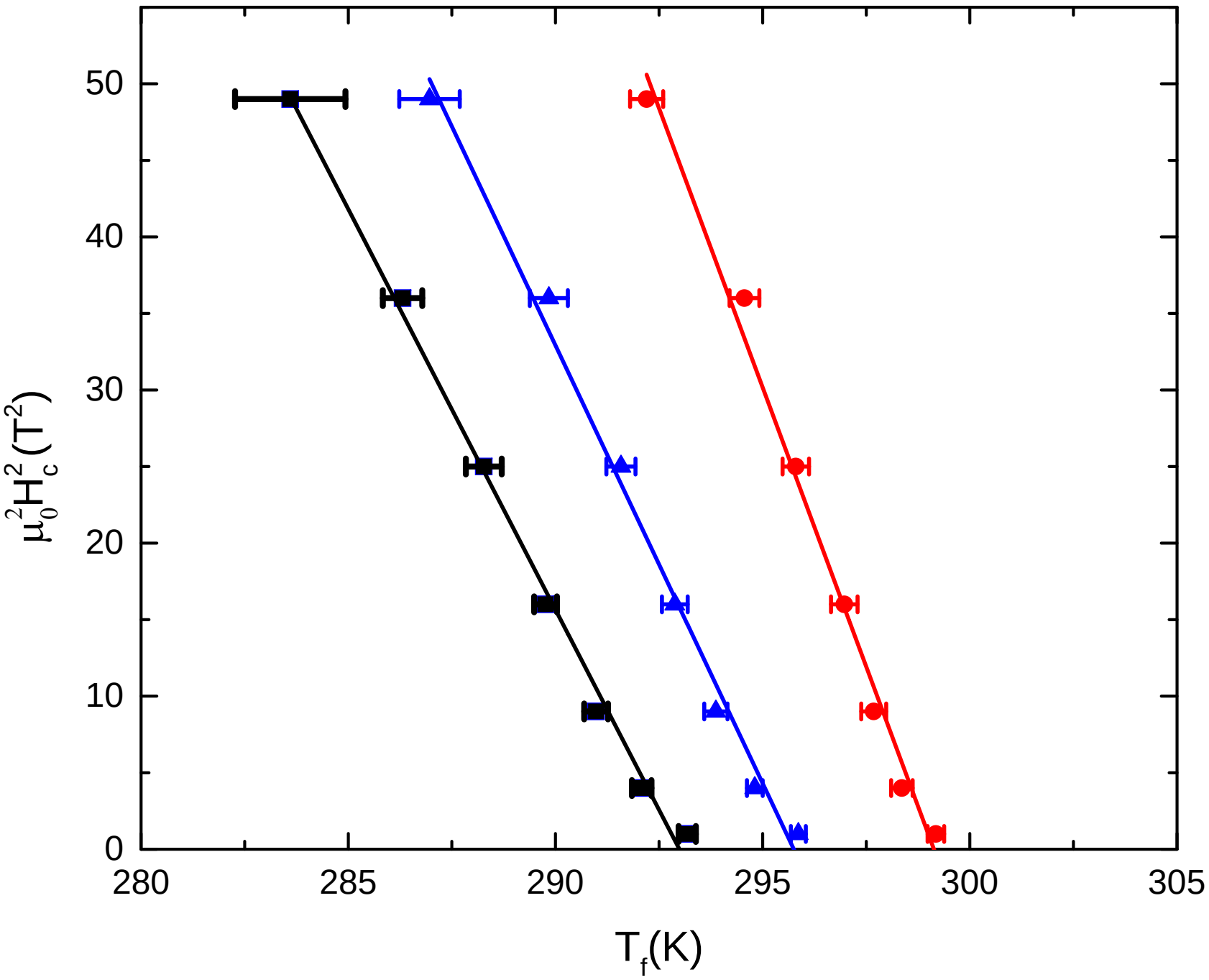

Fig. 3

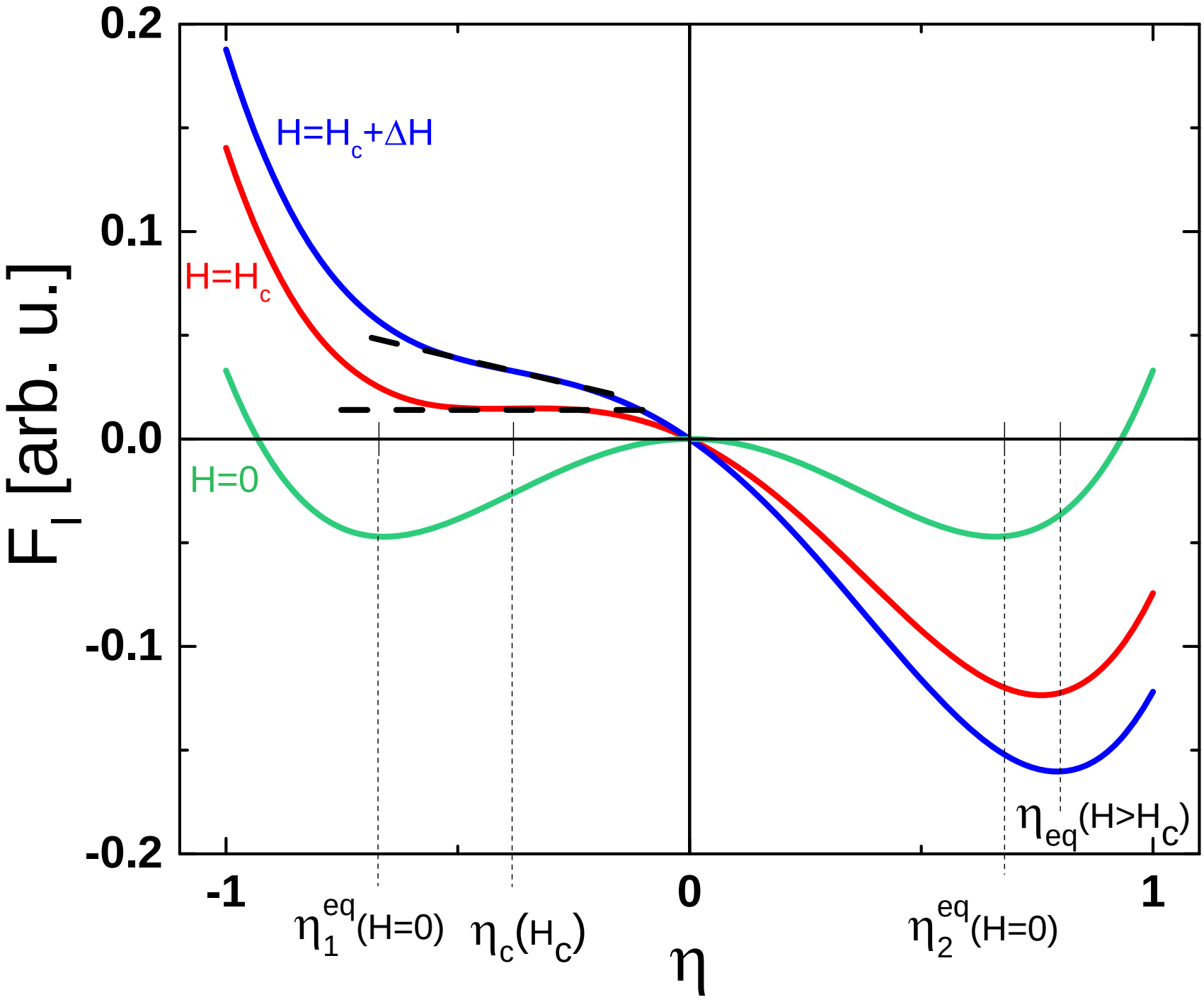
0.2
0.1
0.0
-0.1
-0.2
F_l [arb. u.]
H=H$_c$+ΔH
H=H$_c$
H=0
-1
0
1
η
$\eta_1^{eq}(H=0)$
$\eta_c(H_c)$
$\eta_2^{eq}(H=0)$
$\eta_{eq}(H>H_c)$

Fig. 4

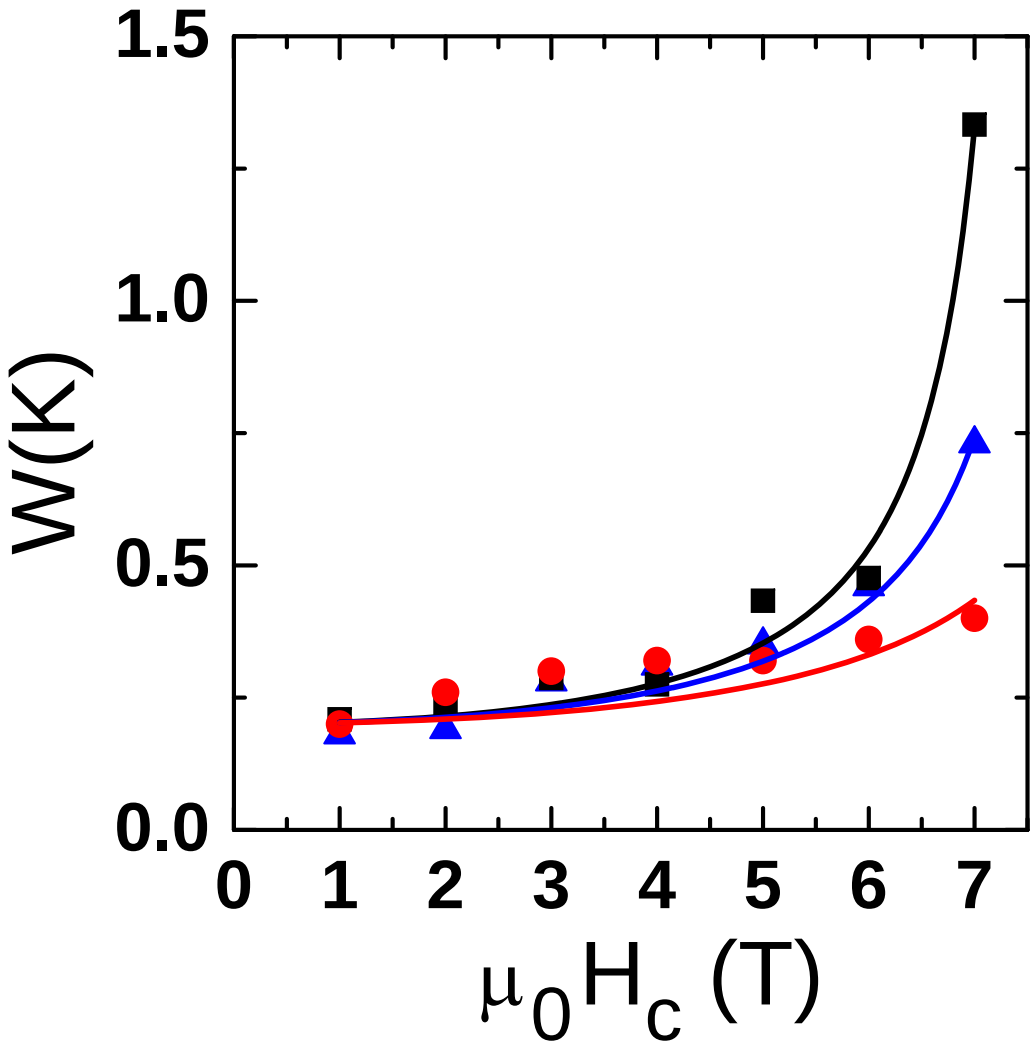

Fig. 5